

## Article

# Multi-Scale Analysis of Grain Size in the Component Structures of Sediments Accumulated along the Desert-Loess Transition Zone of the Tengger Desert and Implications for Sources and Aeolian Dust Transportation

Xinran Yang <sup>1</sup>, Jun Peng <sup>1,2,\*</sup> , Bing Liu <sup>3</sup> and Yingna Liu <sup>2</sup>

<sup>1</sup> School of Earth Sciences and Spatial Information Engineering, Hunan University of Science and Technology, Xiangtan 411201, China; yangxinranhn@163.com

<sup>2</sup> State Key Laboratory of Earth Surface Processes and Resource Ecology, Beijing Normal University, Beijing 100875, China; liuyingna@bnu.edu.cn

<sup>3</sup> Key Laboratory of Desert and Desertification, Northwest Institute of Eco-Environment and Resources, Chinese Academy of Sciences, Lanzhou 730000, China; liubing2014@lzb.ac.cn

\* Correspondence: pengjun10@mails.ucas.ac.cn

**Abstract:** Aeolian sediments accumulated along the desert-loess transition zone of the Tengger Desert include heterogeneous textures and complex component structures in their grain-size distributions (GSD). However, the sources of these aeolian sediments have not been resolved due to the lack of large reference GSD sample datasets from adjacent regions that contain various types of sediments; such datasets could be used for fingerprinting based on grain-size properties. This lack of knowledge hinders our understanding of the mechanism of aeolian dust releases in these regions and the effects of forcing of atmospheric circulations on the transportation and accumulation of sediments in this region. In this study, we employed a multi-scale grain-size analysis method, i.e., a combination of the single-sample unmixing (SSU) and the parametric end-member modelling (PEMM) techniques, to resolve the component structures of sediments that had accumulated along the desert-loess transition zone of the Tengger Desert. We have also analyzed the component structures of GSDs of various types of sediments, including mobile and fixed sand dunes, lake sediments, and loess sediments from surrounding regions. Our results demonstrate that the patterns observed in coarser fractions of sediments (i.e., sediments with a mode grain size of  $>100\ \mu\text{m}$ ) from the transition zone match well with the patterns of component structures of several types of sediments from the interior of the Tengger Desert, and the patterns seen in the finer fractions (i.e., fine, medium, and coarse silts with a modal size of  $<63\ \mu\text{m}$ ) were broadly consistent with those of loess sediments from the Qilian Mountains. The deflation/erosion of loess from the Qilian Mountains by wind was the most important mechanism underlying the production of these finer grain-size fractions. The East Asia winter monsoon (EAWM) played a key role in transportation of the aeolian dust from these source regions to the desert-loess transition zone of the desert.

**Keywords:** grain size; aeolian sediment; single-sample unmixing; end-member modelling; East Asia winter monsoon



**Citation:** Yang, X.; Peng, J.; Liu, B.; Liu, Y. Multi-Scale Analysis of Grain Size in the Component Structures of Sediments Accumulated along the Desert-Loess Transition Zone of the Tengger Desert and Implications for Sources and Aeolian Dust Transportation. *Atmosphere* **2024**, *15*, 239. <https://doi.org/10.3390/atmos15020239>

Academic Editor: Avelino Eduardo Saez

Received: 14 January 2024

Revised: 1 February 2024

Accepted: 5 February 2024

Published: 19 February 2024



**Copyright:** © 2024 by the authors. Licensee MDPI, Basel, Switzerland. This article is an open access article distributed under the terms and conditions of the Creative Commons Attribution (CC BY) license (<https://creativecommons.org/licenses/by/4.0/>).

## 1. Introduction

Aeolian sediments accumulated in arid/semi-arid regions are essential archives for understanding sedimentary and geomorphological processes and their dynamic responses to environmental variation [1]. Grain-size analysis of aeolian samples has been widely applied to investigate their textures and compositions [2,3], sedimentary environments [4–6], potential sources [7–9], and transportation processes [10–12]. The multimodal grain-size distributions (GSDs) of sediments are often regarded as a result of the sorting and mixing of unimodal subpopulations from a range of sources and/or depositional processes [13–15].

Single-sample unmixing (SSU) and parametric end-member modelling (PEMM) of GSDs are two common numerical decomposition techniques used to reveal potential grain-size subpopulations/end-members, and they reveal the component structures of GSDs at different scales [16]. Subpopulations defined by the SSU method are derived from individual GSDs and therefore provide process-related information on individual GSDs and the associated between-sample variability, while end-members defined by the PEMM method are derived from the average component structure shared by all GSDs and therefore represent general states of the grain-size components and the associated between-member variability [16]. However, the combination of these two different methods to investigate the component structure of GSDs has seldom been applied to the grain-size analysis of aeolian sediments.

Studies on aeolian sediments along the desert-loess transition zone of the Tengger Desert have revealed great variability in grain-size characteristics [17–21] and significant complexity in the component structures of GSDs [22,23] due to significant spatial-temporal variations in both wind direction and wind strength across the region and to complex local topographical and hydrological processes. Guan et al. [20] analyzed 56 surface aeolian samples from the desert-loess transition zone of the Tengger Desert and suggested that the coarse-grain-size fraction (61.8–185.4  $\mu\text{m}$ ) had a greater degree of sensitivity to the expansion/retraction of the aeolian system compared to finer fractions. They suggested that the coarse fraction originated from the interior of the Tengger Desert and that finer fractions might have more complicated sources. Peng et al. [22] analyzed a large number of GSDs of aeolian sediments along the transition zone using the SSU method and suggested that these samples consist of at least five distinct components, each representing a different potential source, including both local and distant materials from the upwind Tengger Desert, Qilian Mountains, Hexi Corridor, and Gobi desert system in the Alxa Plateau. However, due to the lack of data that could serve as a basis for fingerprinting, specifically data on the various types of sediments from adjacent regions, their grain-size properties, the conclusions of Peng et al. [22] remain speculative and therefore require validation. Liu et al. [23] analyzed the component structures of various types of surface sediments across the Tengger Desert using the PEMM method. They demonstrated that the abundance of different end-members varied between different sediment types and used end-members with coarser grain sizes to indicate aeolian activity. However, the vast majority of samples analyzed by Liu et al. [23] were collected from the interior of the desert. In conclusion, at this time, no study has been conducted to investigate the similarities/differences between the component structures of aeolian sediments within the desert and those along the transition zone and to reveal the potential linkage between them. The resultant knowledge gap hinders our understanding of the sources and transportation processes of aeolian sediments accumulated along the transition zone of the desert.

In this study, we applied the SSU and PEMM methods to GSDs of aeolian sediments collected from wide regions in both the interior and the transition zone of the Tengger Desert to reveal the potential linkage between their component structures. The degrees of variability in grain-size characteristics, structural compositions, and end-members between various types of sediments were investigated and compared in a systematic manner, and the implications for dust release from adjacent regions and for the sources and transportation of aeolian dust along the transition zone are discussed.

## 2. Materials and Methods

### 2.1. Study Area, Samples, and Grain-Size Measurements

The Tengger Desert, located in the drylands of northern China, is one of the major proximal deserts upwind of the Chinese Loess Plateau (CLP). It provides vast amounts of aeolian dust, which influence the regional environments [17,24,25]. Variability in aridity and winds, together with complex local topographical and hydrological processes, has led to significant temporal and spatial heterogeneity in the accumulation of aeolian sediments around the desert [24]. The desert, located in the margin of the East Asia summer monsoon

(EASM), is a sedimentary basin facilitating sediment accumulation by carrying clastic sediments, clay-sized particles, and fine silts from the mountains around the desert to piedmonts and foreland basins [24]. The climate of the area is dominated by the EASM in the summer and by the East Asia winter monsoon (EAWM) in the winter. In this study, a total of 486 samples of various types were collected from sites representing wide regions in and surrounding the desert (Figure 1), including (1) sediments from mobile, semi-mobile, and fixed/semi-fixed dunes; interdune depressions; nabkhas; and interdune lakes from the interior of the desert [23]; (2) loess from the northern piedmont of the eastern Qilian Mountains in the southwest of the desert; and (3) aeolian sand and sandy loess from the desert-loess transition zone at the southern margin of the desert [22,24,25].

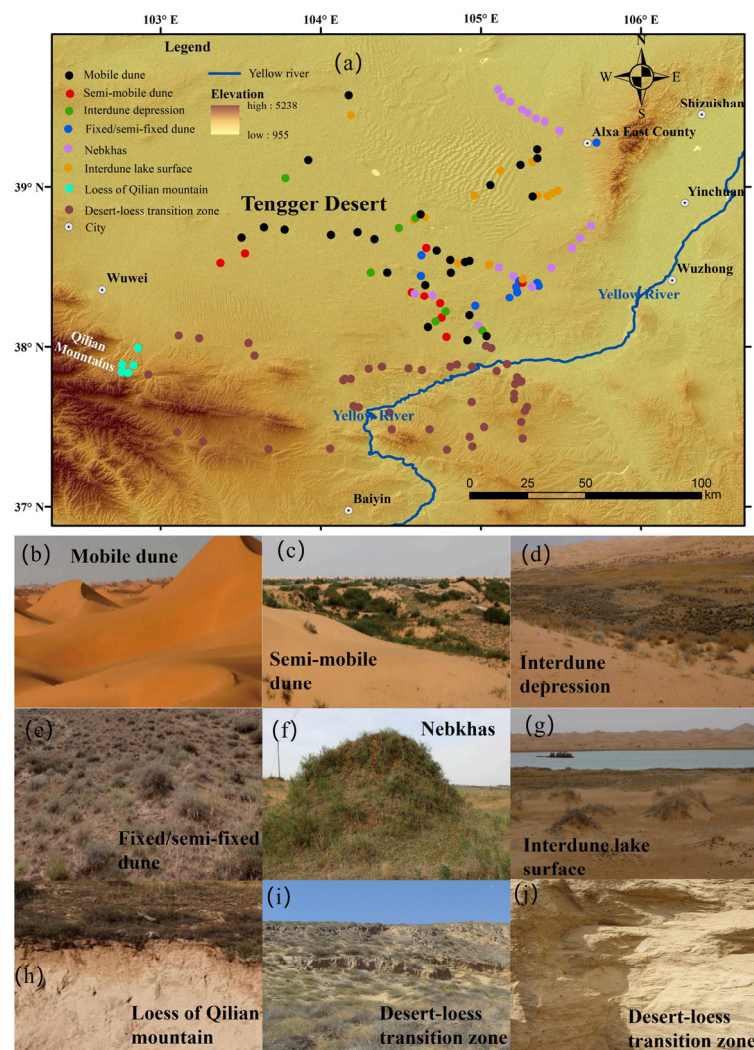


**Figure 1.** (a) grain-size sampling sites around the Tengger Desert. Different types of sediments are shown in different colors. (b–j) representative photos of sampling sites for various types of sediments, including (b) mobile dunes, (c) semi-mobile dunes, (d) interdune depressions, (e) fixed/semi-fixed dunes, (f) nabkhas, (g) interdune lake surfaces, (h) loess from the Qilian Mountains, (i,j) sediments from the desert-loess transition zone.

Grain-size measurements were conducted at Hunan University of Science and Technology. Bulk samples (~0.65 g) were pretreated with 10% HCl to remove carbonate and 30% H<sub>2</sub>O<sub>2</sub> to remove organic matter. Then, the samples were further treated with 10% (NaPO<sub>3</sub>)<sub>6</sub> in an ultrasonic bath and subsequently measured using a Malvern Mastersizer 2000 particle size analyzer. Repeated measurements suggest that the measured GSDs are characterized by a relative standard deviation of less than 3%.

### 2.2. Description Statistics

Descriptive statistics such as the mean grain size ( $\mu$ ), standard deviation ( $\sigma$ ), skewness ( $S$ ), and kurtosis ( $K$ ) of measured GSDs were calculated according to Folk and Ward [13] as follows:

$$\mu = \frac{\Phi_{16} + \Phi_{50} + \Phi_{84}}{3} \tag{1}$$

$$\sigma = \frac{\Phi_{84} - \Phi_{16}}{4} + \frac{\Phi_{95} - \Phi_5}{6.6} \tag{2}$$

$$S = \frac{\Phi_{84} + \Phi_{16} - 2\Phi_{50}}{2(\Phi_{84} - \Phi_{16})} + \frac{\Phi_{95} + \Phi_5 - 2\Phi_{50}}{2(\Phi_{95} - \Phi_5)} \tag{3}$$

$$K = \frac{\Phi_{95} - \Phi_5}{2.44(\Phi_{75} - \Phi_{25})} \tag{4}$$

where  $\Phi_5, \Phi_{16}, \Phi_{25}, \Phi_{50}, \Phi_{75}, \Phi_{84}, \Phi_{95}$  ( $\Phi = -\log_2 D$  and  $D$  is the grain size level in unit  $\mu\text{m}$ ) represent the grain sizes corresponding to cumulative percentage volumes of 5%, 16%, 25%, 50%, 75%, 84%, and 95% of the measured GSD, respectively. The classification of samples as clay (0–4  $\mu\text{m}$ ), silt (4–63  $\mu\text{m}$ ), and sand (>63  $\mu\text{m}$ ) used in this study followed [26].

### 2.3. Single-Sample Unmixing

The SSU method optimizes the following residual sum of squares (RSS) to obtain the optimal set of parameters describing a GSD:

$$RSS = \sum_{i=1}^{i=n} (y_i - \hat{y}_i)^2 = \sum_{i=1}^{i=n} \left( y_i - \sum_{j=1}^{j=k} g(x_i, \theta_j) \right)^2 \tag{5}$$

where  $x_i$  is the  $i$ -th grain-size level,  $y_i$  and  $\hat{y}_i$  represent respectively the  $i$ -th measured and fitted grain-size volume percentages (a GSD is defined as the variation in  $y_i$  as a function of  $x_i$  for a series of  $i$  indices ranging from 1 to 101);  $n$  is the total number of measured grain-size levels;  $\theta_j$  is the parameters of the  $j$ -th subpopulation;  $g(x_i, \theta_j)$  is a probability density function describing a grain-size subpopulation with a set of parameters  $\theta_j$  at a grain-size level  $x_i$ ; and  $k$  is the total number of subpopulations used for unmixing a GSD.

In this study, we used the transformed skew normal function to describe a grain-size subpopulation as follows [16]:

$$g(x, \theta) = g(x, x_m, v_m, \alpha, \omega) = v_m \exp\left(-\frac{(2D + x - x_m)(x - x_m)}{2\omega^2}\right) \frac{1 + \operatorname{erf}\left(\frac{\alpha(x - x_m + D)}{\sqrt{2}\omega}\right)}{1 + \operatorname{erf}\left(\frac{\alpha D}{\sqrt{2}\omega}\right)} \tag{6}$$

$$D = \omega \left( \sqrt{\frac{2\alpha^2}{\pi(1 + \alpha^2)}} - \sqrt{1 - \frac{2\alpha^2}{\pi(1 + \alpha^2)}} \frac{4 - \pi}{4} \left( \frac{2\alpha^2}{\pi + (\pi - 2)\alpha^2} \right)^{\frac{3}{2}} - \frac{1}{2} \exp\left(-\frac{2\pi}{|\alpha|}\right) \operatorname{sign}(\alpha) \right) \tag{7}$$

$$\operatorname{erf}(x) = \frac{2}{\sqrt{\pi}} \int_0^x \exp(-t^2) dt \tag{8}$$

The parameters of a subpopulation are  $\theta = \{x_m, v_m, \alpha, \omega\}$ . The transformed function contains two free parameters specifying the peak position ( $x_m$ ) and magnitude ( $v_m$ ) of a grain-size subpopulation and can be more easily initialized and constrained during the application of the SSU method [16]. The fitting quality of the model is measured with the figure-of-merit statistic [27]:

$$\text{FOM} = \frac{\sum_{i=1}^{i=n} |y_i - \hat{y}_i|}{\sum_{i=1}^{i=n} |\hat{y}_i|} \times 100\% \tag{9}$$

The degree of overlap between two adjacent grain-size subpopulations is calculated as follows [22]:

$$r = \frac{X_1 - X_2}{\delta_1 + \tau_2} \tag{10}$$

where  $X_1$  and  $X_2$  are the grain-size levels corresponding to the maximum volume percentages of two adjacent subpopulations;  $\delta_1$  is the half-width on the right side of the first subpopulation; and  $\tau_2$  is the half-width on the left side of the second subpopulation. The un-normalized proportion  $p$  (which was later normalized to sum up to 100% to obtain the abundance), the mean grain size  $\mu$  and associated standard deviation  $\sigma$  for a subpopulation are calculated as follows:

$$p = \frac{\sqrt{2\pi}\omega v_m}{\exp(-\frac{D^2}{2\omega^2})(1 + \operatorname{erf}(\frac{\alpha D}{\sqrt{2}\omega}))} \tag{11}$$

$$\mu = x_m - D + \alpha\omega\sqrt{\frac{2}{\pi(1 + \alpha^2)}} \tag{12}$$

$$\sigma = \omega\sqrt{1 - \frac{2\alpha^2}{\pi(1 + \alpha^2)}} \tag{13}$$

The unmixing results of a GSD contain several subpopulations, each of which has its own parameters:  $p$ ,  $\mu$ , and  $\sigma$ . As a result, the unmixed results for a large number of GSDs will contain large sets of parameters for individual subpopulations from a large number of samples. We used the variance-included finite mixture model [28] to classify the pooled unmixed mean grain sizes ( $\mu$ ) by taking the standard deviation ( $\sigma$ ) of subpopulations into account [22]. The optimal number of clusters was determined using the Bayesian information criterion of Schwartz [29]. The unmixing and statistical analysis were implemented using the efficient and flexible R program “ussGSD” [22] which is freely available at the GitHub repository <https://github.com/pengjunUCAS/ussGSD>, accessed on 1 December 2023.

#### 2.4. Parametric End-Member Analysis

The PEMM method tries to minimize the difference between the measured GSDs ( $\mathbf{X}$ ) and the modelled GSDs ( $\hat{\mathbf{X}}$ ).  $\mathbf{X}$  and  $\hat{\mathbf{X}}$  are  $m \times n$  matrices ( $m$  is the number of GSDs and  $n$  the number of grain-size levels).  $\hat{\mathbf{X}}$  can be described by the matrix product of abundances ( $\mathbf{M}$ ) and end-members ( $\mathbf{B}$ ) [30], as follows:

$$\hat{\mathbf{X}} = \mathbf{M}\mathbf{B} \tag{14}$$

where  $\mathbf{M}$  is a  $m \times k$  matrix ( $k$  is the number of end-members) of numbers that are nonnegative and constrained such that the sum of the entries in each row is equal to 100%.  $\mathbf{B}$  is a  $k \times n$  matrix that can be described as follows:

$$\mathbf{B} = \begin{pmatrix} f(x_1, \varphi_1) & f(x_2, \varphi_1) & \dots & f(x_n, \varphi_1) \\ f(x_1, \varphi_2) & f(x_2, \varphi_2) & \dots & f(x_n, \varphi_2) \\ \vdots & \vdots & \ddots & \vdots \\ f(x_1, \varphi_k) & f(x_2, \varphi_k) & \dots & f(x_n, \varphi_k) \end{pmatrix} \tag{15}$$

where  $\varphi_j$  is the parameters of the  $j$ -th subpopulation and  $f(x_i, \varphi_j)$  is a probability density function describing a grain-size subpopulation with a set of parameters  $\varphi_j$  at grain-size level  $x_i$ . The transformed skew normal function describing an end-member is as follows [16]:

$$f(x, \varphi) = f(x, x_m, \alpha, \omega) = \frac{1}{\sqrt{2\pi}\omega} \exp\left(-\frac{(x - x_m + D)^2}{2\omega^2}\right) \left(1 + \operatorname{erf}\left(\frac{\alpha(x - x_m + D)}{\sqrt{2}\omega}\right)\right) \tag{16}$$

The parameters of a subpopulation are  $\varphi = \{x_m, \alpha, \omega\}$ .  $D$  is an intermediate quantity described by Equation (7). In this study, the PEMM method was implemented using the R function “PEMM” [16]. The difference between the measured GSDs and the fitted values was measured using the mean of the angles (and the mean of squared Pearson correlation coefficients) of the row vectors of matrices  $\mathbf{X}$  and  $\hat{\mathbf{X}}$ .

### 3. Results

#### 3.1. Grain-Size Characteristics

We summarized the volume percentages of clay, silt, and sand fractions for different types of sediments using a ternary plot (Figure 2). The plot shows that for samples of mobile and semi-mobile dunes, and for most samples of interdune depressions, sand content was greater than 96%, silt content was lower than 3.4%, and clay content was lower than 0.6%. For most samples of fixed/semi-fixed dunes and nabkhas, sand content was greater than 80%, silt content was lower than 15%, and clay content was lower than 5%. Samples from interdune lake surfaces had greater contents of silt and clay and lower content of sand compared to samples of mobile and semi-mobile dunes, interdune depressions, fixed/semi-fixed dunes and nabkhas. By contrast, most samples of loess from the Qilian Mountains had sand content less than 15%, silt content greater than 75%, and silt content less than 10%. For samples from the transition zone, the content of sand (from 3% to 99%) and silt (from less than 1% to 80%) varied widely, while the content of clay was less than 17%, suggesting that these samples demonstrated the greatest variability in the contents of clay, silt, and sand compared to other types of sediments.

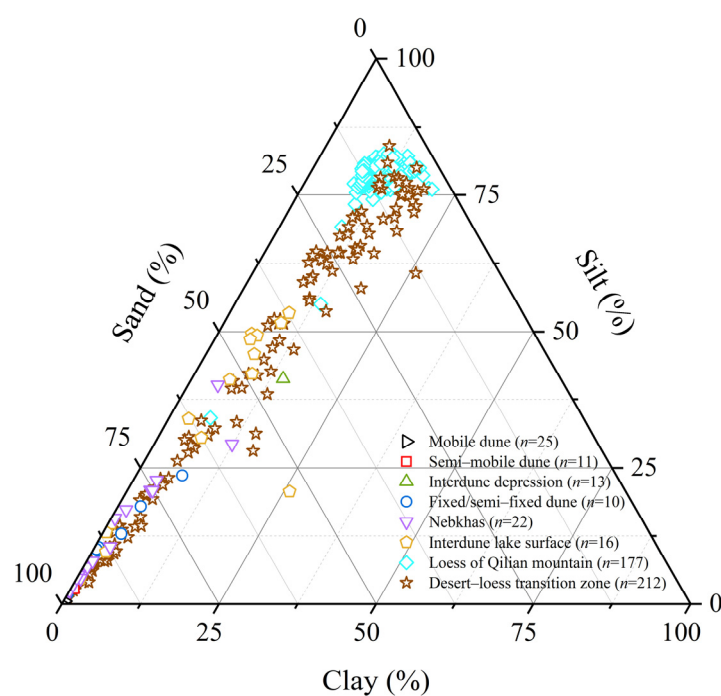


**Figure 2.** Ternary plot showing abundances of clay, silt, and sand for various types of sediments.

The relationships between standard deviation (in unit  $\Phi$ ), skewness, and mean grain size (in unit  $\Phi$ ) among various types of sediments differed (Figure 3). For samples from mobile and semi-mobile dunes and interdune depressions, the variation in sorting (standard deviation) and skewness as a function of the mean size was not significant. The mean sizes were smaller than  $3\Phi$ . The standard deviation and skewness of most samples were centered at  $0.5\Phi$  and 0, respectively, suggesting good sorting and symmetry. For samples from fixed/semi-fixed dunes and nabkhas, the sorting and skewness were positively correlated with the grain size; the sorting increased and the skewness decreased as the mean size became coarser. For samples from the interdune lake surfaces, the sorting was positively

correlated with the mean size. However, the variation in skewness as a function of mean size did not follow a uniform pattern. For almost all samples of loess from the Qilian Mountains, the sorting was positively correlated with the mean size, but the skewness was negatively corrected with the mean size. Samples from the transition zone demonstrated the greatest variability in the patterns of correlation between the mean size and the other two statistics.

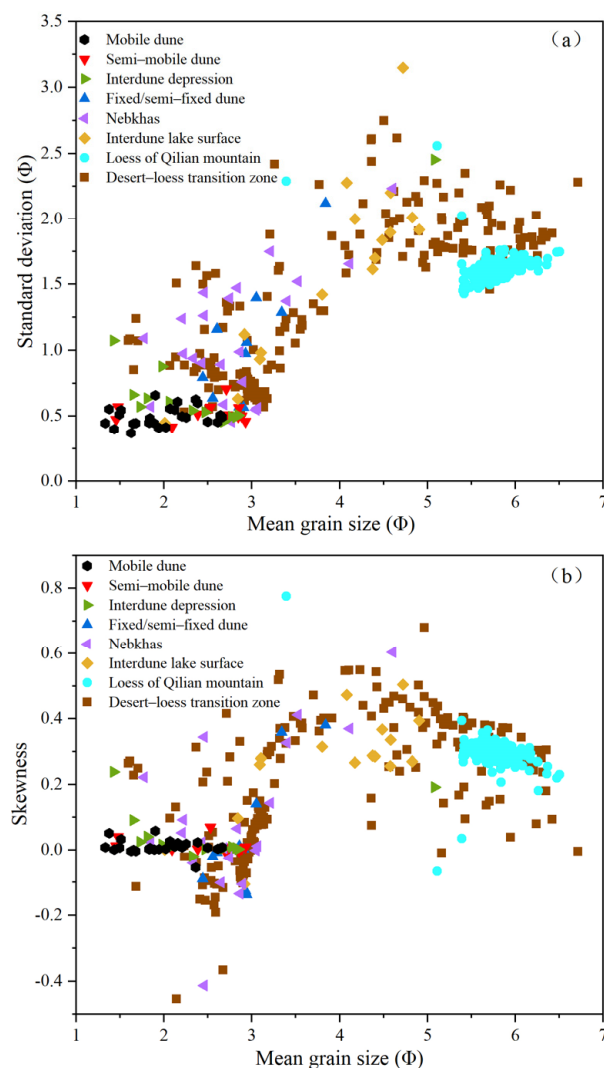


**Figure 3.** Variations in (a) sorting and (b) skewness as a function of mean grain size for various types of sediments.

### 3.2. Structural Compositions

The SSU results for representative GSDs of various types of sediments are presented in Figure 4. The FOM values were smaller than 5%. For GSDs unmixed with more than one subpopulation, the minimum degree of overlapping between adjacent subpopulations was greater than 0.7, indicating the unmixing results were acceptable. The distributions of the unmixed grain-size means of various types of sediments are shown as a (simplified) radial plot [31] in Figure 5. For samples from mobile dunes, the pooled unmixing results could be clustered only as one group (Figure 5a). Samples from semi-mobile dunes and interdune depressions could be best described by two clusters (Figure 5b,c). Samples of fixed/semi-fixed dunes, nebkhas, and loess from the Qilian Mountains were described by four clusters (Figure 5d,e,g). Samples from the interdune lake surfaces and the transition zone formed five distinct clusters (Figure 5f,h).

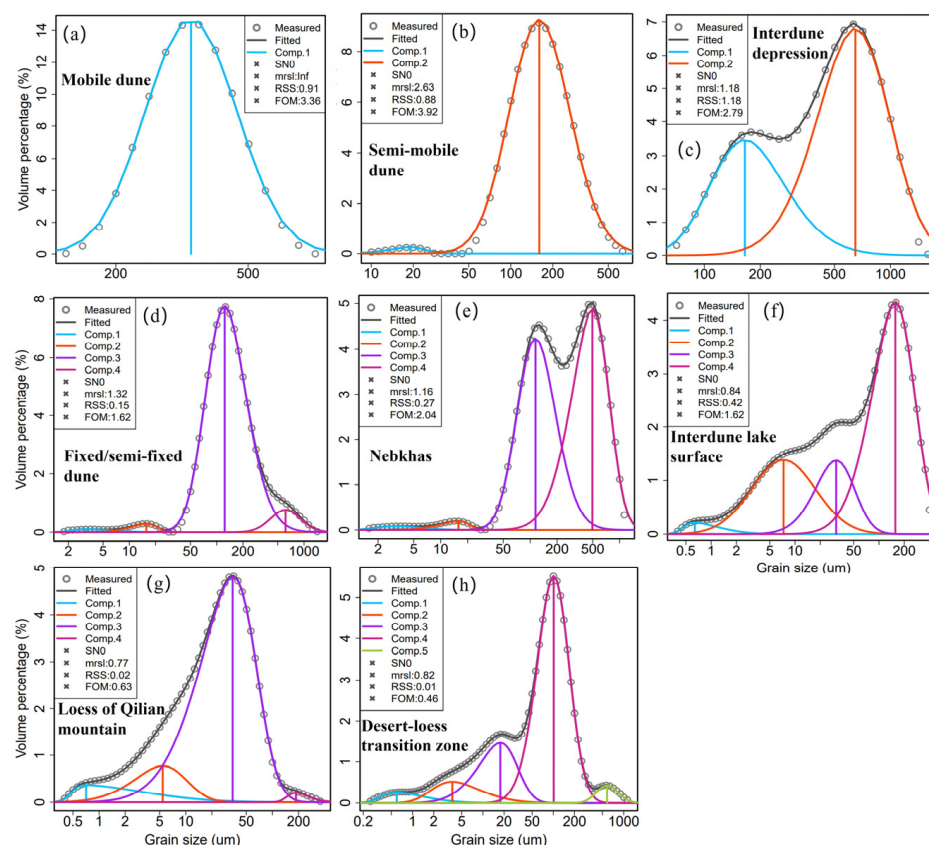


**Figure 4.** SSU results of grain-size distribution for various types of sediments, using the skew normal distribution. “SN0” is the transformed skew normal distribution; “mrsI” is the minimum degree of overlapping between adjacent subpopulations; “RSS” and “FOM” are the residual sum of squares and the figure-of-merit value, respectively. Note that the  $x$ -axis is plotted on a log scale for better visualization.

We compared the clustering results, including the mean grain size and the normalized abundance of individual clusters, between various types of sediments; the results are presented in Figure 6. Almost all types of sediments (except loess from the Qilian Mountains) predominantly contained a coarse subpopulation in the size range 100–250  $\mu\text{m}$ . The abundance of this coarse fraction decreased gradually as the sediment types changed from mobile and semi-mobile dunes to interdune depressions, fixed/semi-fixed dunes, and nebkhas. In addition, samples from fixed/semi-fixed dunes, nebkhas, interdune lake surfaces, and desert-loess transition zone contained an extremely coarse fraction in the interval of 500–1000  $\mu\text{m}$ . Samples of fixed/semi-fixed dunes and nebkhas demonstrated very similar structural compositions. The structural compositions of samples from interdune lake surfaces and transition zone were also relatively consistent. Samples from fixed/semi-fixed dunes, nebkhas, interdune lake surfaces, loess from the Qilian Mountains, and the transition zone contained two subpopulations in the size range 2–32  $\mu\text{m}$ . In addition, samples from interdune lake surfaces, loess from the Qilian Mountains, and transition zone contained a clay fraction.

### 3.3. End-Member Variations

The distributions of end-members of various types of sediments are presented in Figure 7. The optimized mean angles between the measured and modelled GSDs for various types of sediments were smaller than  $5^\circ$ , indicating good fit quality. Sediments of mobile and semi-mobile dunes were modelled using four closely overlapping end-members, suggesting that the PEMM algorithm had an intrinsic tendency to generate extra end-members only within grain-size intervals associated with larger volume percentages

as the number of end-members increased, as pointed out by Peng et al. [16]. Loess from the Qilian Mountains also yielded four end-members, but they were significantly much finer. By contrast, the remaining types of sediments yielded at least five end-members.

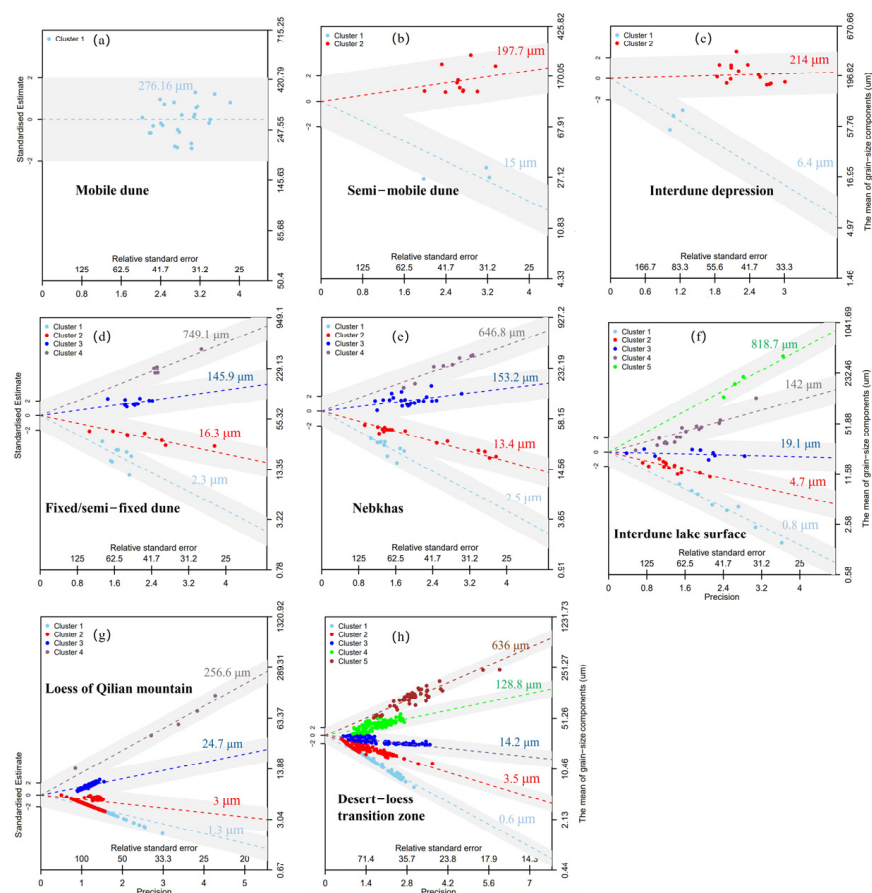


**Figure 5.** Simplified radial plots showing the classification of the means of grain-size components extracted from the pooled unmixing results using the finite mixture model-based Bayesian clustering algorithm [22] for various types of sediments, including (a) mobile dunes, (b) semi-mobile dunes, (c) interdune depressions, (d) fixed/semi-fixed dunes, (e) nebkhas, (f) interdune lake surfaces, (g) loess from the Qilian Mountains, (h) sediments from the desert-loess transition zone. The gray region indicates the two-sigma range of a cluster.

Comparisons of the modal size and the corresponding abundance of end-members of various types of sediments are presented in Figure 8. Sediments from mobile and semi-mobile dunes and interdune depressions contained large fractions of fine-to-coarse sand and those from fixed/semi-fixed dunes were dominated by a fine-sand fraction. Sediments from nebkhas, interdune lake surfaces, and the desert-loess transition zone contained non-negligible fractions of silt and various sands. The modal numbers of end-members decreased gradually between samples from mobile dune and sediments from interdune lake surfaces. The modal sizes of all four end-members for loess from the Qilian Mountains represented silt fractions, suggesting that their sources were intrinsically different from those of sediments from the interior of the desert. In addition, a comparison of the SSU and PEMM results (Figures 6 and 8) suggested that the clusters of subpopulations derived by the SSU method are distributed more evenly across the grain-size scales, while the PEMM end-members fall within much narrower grain-size intervals, suggesting that SSU has a greater capacity to recognize independent grain-size components as compared to PEMM [22].

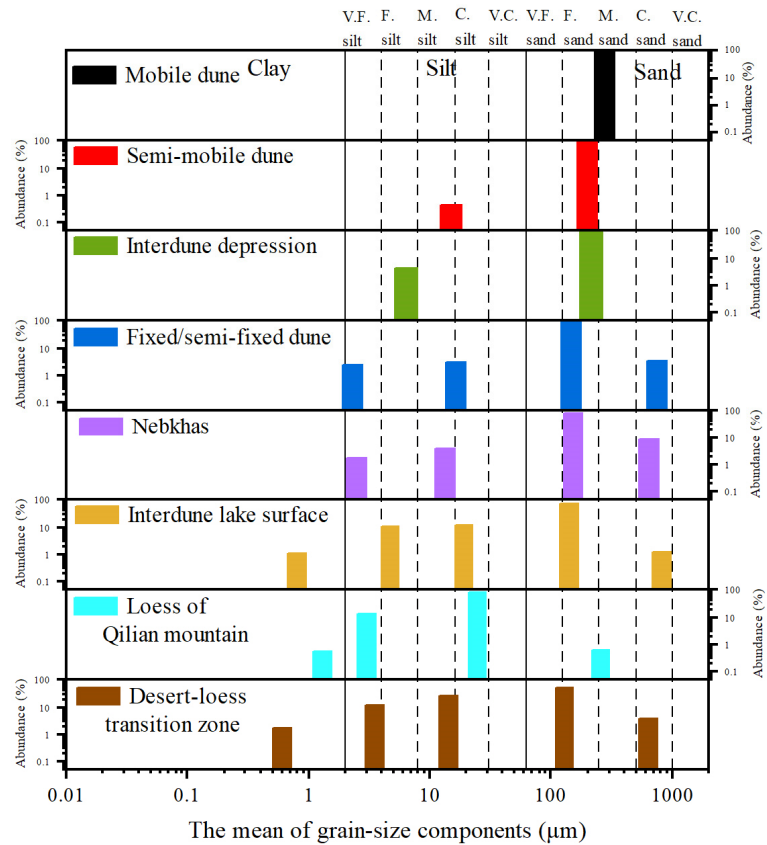


**Figure 6.** Comparison of the means and abundances for clusters of grain-size components classified using the finite mixture model-based Bayesian clustering algorithm [22] for various types of sediments. Note that the  $y$ -axis is plotted on a log scale for better visualization.

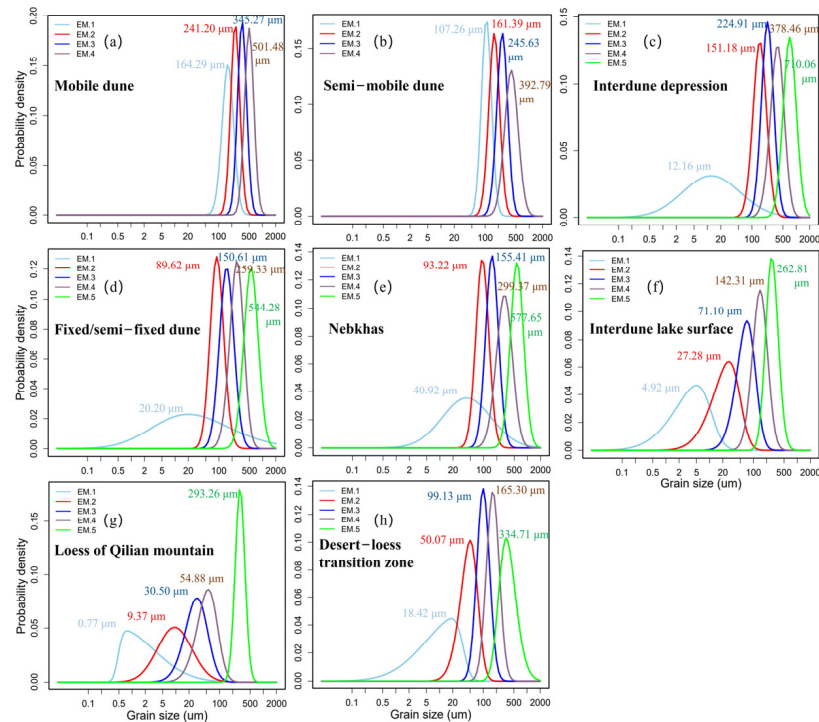


**Figure 7.** Variations of probability density distributions of end-members for various types of sediments. Note that the  $x$ -axis is plotted on a log scale for better visualization.

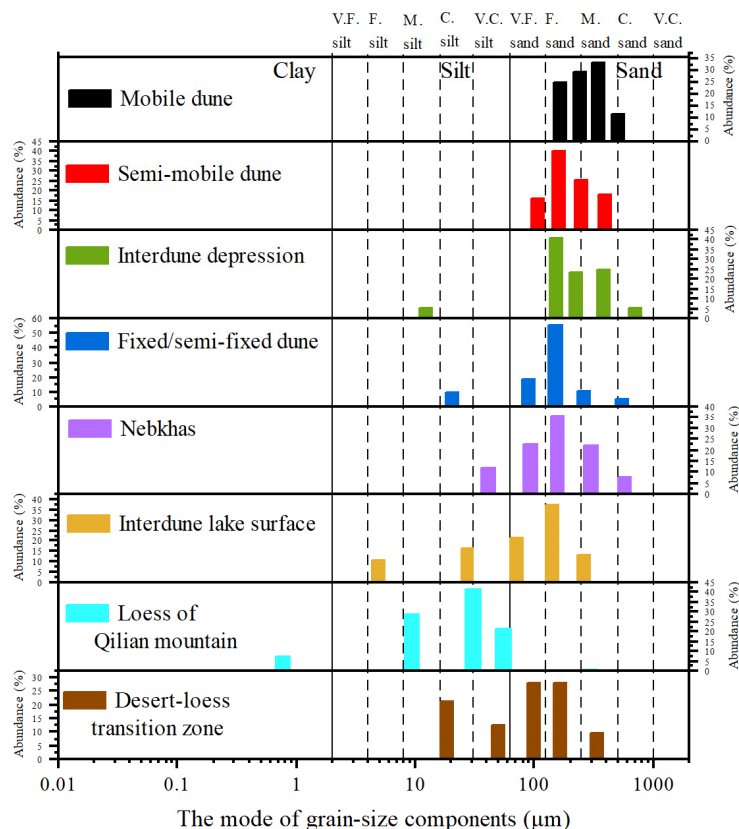


**Figure 8.** Comparison of the modal sizes and abundances of end-members for various types of sediments.

#### 4. Discussion

##### 4.1. Implication for Sources of Aeolian Sediments from the Desert-Loess Transition Zone

The proportions of clay, silt, and sand (Figure 2), the mean grain size, the sorting, and the skewness of the GSDs (Figure 3) are different between various types of sediments. Data points representing six types of sediments from the interior of the desert and loess from the northern piedmont of the eastern Qilian Mountains cover only certain parts of the ternary plot in Figure 2 and the scatterplot in Figure 3. By contrast, data points representing aeolian sediments from the desert-loess transition zone cover almost the whole of both plots. Thus, it can be seen that aeolian sediments from the transition zone have the greatest grain-size variability and that they inherit the grain-size characteristics of all other types of sediments. These lines of evidence imply that their GSDs formed as an admixture of various sources of sediments, a finding in accordance with conclusions drawn from previous studies [22,23].

The SSU and PEMM methods that reveal grain-size component structures on different scales were used to analyze various types of sediments (see Figures 6 and 8). For aeolian sediments from the transition zone, the first three clusters of subpopulations defined by the SSU method (with mean sizes of 0.6 µm, 3.5 µm, and 14.2 µm) are closely related to the first two clusters of samples from fixed/semi-fixed dunes and nebkhas and the first three clusters of samples from interdune lake surfaces and loess from the Qilian Mountains (Figure 6). In addition, for aeolian sediments from the transition zone, the first two end-members defined by the PEMM method (with modal sizes of 18.4 µm and 50.1 µm) can be broadly associated with certain end-members of samples from interdune lake surfaces within the Tengger Desert and loess from the Qilian Mountains (Figure 8). These results suggest that the sources of the finer fractions of aeolian sediments in the transition zone may be the Qilian Mountains and the Tengger Desert. Such finer grain-size fractions have been reported from loess sediments from various regions [7,32–35].

There is debate on the production of these finer grain-size fractions (fine, medium, and coarse silts). Crouvi et al. [36] proposed aeolian abrasion as an important mechanism for the production of coarse silt quartz grains. Amit et al. [37] revealed a genetic association between the coarse silt fraction of the loess in CLP and the primary production of coarse silt in the proximal Mu Us, Tengger, and Badain Jaran deserts and suggested that coarse silts in the loess of CLP were produced by abrasion of quartz sand within these deserts. On the other hand, the empirical findings of Swet et al. [38] suggested that less dust was generated by sand abrasion than by the removal of clay minerals coated on sand-grain surfaces and that non-sandy soils were the major source of dust. Guan et al. [20] found that the Tengger Desert is not the main source area for the silt grain component of size 18.2–61.8  $\mu\text{m}$  identified in sediments from the transition zone. Liu et al. [23] identified a PEMM end-member characterized by a modal size of 28.3  $\mu\text{m}$  in their GSDs, which were collected from the interior of the Tengger Desert, and suggested that the component originated from distant source areas rather than from local regions. We demonstrated that the finer grain-size fractions in aeolian sediments from the transition zone could be most easily associated with loess in the Qilian Mountains, which contained a large amount of silt (see Figures 6 and 8). Loess sediments were widely distributed along the Qilian Mountains. Their accumulation started as early as 0.83–0.85 Ma ago, and they reached a maximum thickness of >200 m [39,40]. Many studies [41–43] have suggested that sediments along the Qilian Mountains might have been a major source of silts deposited on the western part of the CLP. Considering that the transition zone is located between the desert and the CLP, the Qilian Mountains should also be an important source of the finer grains accumulated there. Accordingly, we suggest that the deflation/erosion of loess from the Qilian Mountains by wind was the most important mechanism underlying the production of these finer grain-size fractions (see Section 4.2). Interdune lake surfaces within the Tengger Desert were the second potential source for the finer grain-size fractions, although they contain less silt compared to the loess in the Qilian Mountains (Figures 6 and 8).

For all types of sediments collected from the interior of the desert, clusters of SSU subpopulations with coarser mean sizes are generally consistent with those of sediments from the transition zone, which have a mean size of 128.8  $\mu\text{m}$  (fine sand) (Figure 6). For sediments from the transition zone, the fifth subpopulation cluster, with a mean size of 636  $\mu\text{m}$  (coarse sand), matches the last subpopulation clusters for fixed/semi-fixed dunes, nebkhas, and sediments from interdune lake surfaces. In addition, PEMM end-members with coarser mean sizes are found in all types of sediments collected from the interior of the desert, but they are absent from loess from the Qilian Mountain (Figure 8). Grain-size components with such coarser mean sizes have been reported in many dune fields in northern China [3,4,9] and they can be transported only over short distances. These points suggest that the only source of the coarser grain-size fractions accumulated in the transition zone is the interior of the Tengger Desert, which is adjacent and located in the upwind direction. A proximal supply of coarse-grained dust upwind has been reported not only from sand/dune fields in northern China, such as the Mu Us Desert [44], Qinghai Lake basin [4], and the Kumtagh Desert [9], but also from aeolian sediments worldwide, for example, in aeolian/loess sediments from the Mediterranean [45], Egypt [46], and Israel [36].

#### 4.2. Implications for Aeolian Dust Transportation

The first two SSU clusters, with central means of 0.6  $\mu\text{m}$  and 3.5  $\mu\text{m}$  (not identified by the PEMM method), have been widely reported in aeolian sediments from northern China [19,32]. The enrichment of clay and very fine silt can result from pedogenesis and weathering of finer grains, such as primary loess [47]. According to Pye [48], aeolian grains with a diameter <20  $\mu\text{m}$  can be carried by the wind up to thousand kilometers. Their presence can be related to long-term inputs originating from both local and distant fluvial, lacustrine, and pedogenic components [24] and carried by local wind regimes and the

upper-level westerlies; they can also be the result of the aggregation/adhering of fine particles to larger ones [49].

The EAWM is the main transporting force for loess sediments in the CLP [44]. The desert-loess transition zone of the Tengger Desert is upwind of the CLP, and it is also controlled by the East Asian monsoon system [17,24]. The SSU cluster with a mean size of 14.2  $\mu\text{m}$  and the PEMM cluster with modal sizes of 18.4  $\mu\text{m}$  and 50.1  $\mu\text{m}$  are associated with typical loess sediments from northern China [32,34,35]. Aeolian grains with diameters ranging between 20  $\mu\text{m}$  and 70  $\mu\text{m}$  are suspended above the surface in the short-term [48]. Loess-like sediments consisting mainly of silt can be transported from the Qilian Mountains to the transition zone through the EAWM. During the winter and spring, the dominant near-surface wind direction along the desert margin is from the northwest [19,50], which causes frequent dust storms as a result of the dry conditions that are typical during these months. Sedimentologic evidence of strengthened EAWM and enhanced release of aeolian dust has been identified in several sites around the south margin of the Tengger Desert [17,23,25].

The SSU cluster with a mean size of 128.8  $\mu\text{m}$  and the PEMM clusters with modal sizes of 99.1  $\mu\text{m}$ , 165.3  $\mu\text{m}$ , and 334.7  $\mu\text{m}$  can be transported only by extremely strong near-surface winds in saltation or creep mode. For example, Guan et al. [51] suggested that a grain-size fraction between 209  $\mu\text{m}$  and 550  $\mu\text{m}$  identified from the Shagou loess section in the southwest margin of the Tengger Desert is an indication that severe sandstorms occurred in the desert during the last interglacial period. It has been widely recognized that strong near-surface winds of this kind can be triggered by strong EAWM events [51,52]. Lastly, considering that fluvial strata are widely distributed along the southern margin of the desert, the SSU cluster with a mean size of 636  $\mu\text{m}$  may originate from the reworking of near-source intermittent fluvial sediments and/or transportation of very coarse sand from the desert by extremely strong sandstorms [24].

## 5. Conclusions

A combination of the SSU and PEMM methods has been used to resolve the component structures of sediments within and surrounding the desert-loess transition zone of the Tengger Desert. The SSU method has greater capacity to identify independent grain-size components compared to the PEMM method. Aeolian sediments accumulated along the transition zone are formed as an admixture of various types of sediments. The coarser and finer grain-size fractions resemble (inherit) characteristics and component structures of sand sediments from the interior of the Tengger Desert and loess sediments from the Qilian Mountains, respectively. The coarser grain-size fractions have proximal sources and are transported downwind from the interior of the desert through strong EAWM events and extremely strong sandstorms, while the finer grain-size fractions are mainly transported from the Qilian Mountains through continuous EAWM during the winter and spring. By contrast, significant contribution of silts from the interior of the Tengger Desert is demonstrated only in sediments from interdune lake surfaces.

**Author Contributions:** Conceptualization, J.P.; methodology, J.P.; software, J.P.; validation, B.L.; formal analysis, X.Y.; investigation, Y.L.; resources, Y.L.; data curation, B.L.; writing—original draft preparation, X.Y.; writing—review and editing, J.P.; visualization, X.Y.; supervision, J.P. All authors have read and agreed to the published version of the manuscript.

**Funding:** This research was funded by the State Key Laboratory of Earth Surface Processes and Resource Ecology, Beijing Normal University (Grant No. 2023-KF-05) and the National Natural Science Foundation of China (Grant No. 41701004).

**Institutional Review Board Statement:** Not applicable.

**Informed Consent Statement:** Not applicable.

**Data Availability Statement:** All data that support the findings of this study are available from the corresponding author on reasonable request.

**Conflicts of Interest:** The authors declare no conflict of interest.

## References

1. Yang, X.P.; Scuderi, L.; Paillou, P.; Liu, Z.T.; Li, H.W.; Ren, X.Z. Quaternary environmental changes in the drylands of China—A critical review. *Quat. Sci. Rev.* **2011**, *30*, 3219–3233. [[CrossRef](#)]
2. Zhang, Z.C.; Dong, Z.B. Grain size characteristics in the Hexi Corridor Desert. *Aeolian Res.* **2015**, *18*, 55–67. [[CrossRef](#)]
3. Li, Z.J.; Wang, F.; Luo, C.W.; Liu, C.Y.; Wang, X.; Yang, S.L.; Ayyamperumal, R.; Zhang, J.H.; Li, B.F.; Fan, Y.X. Enhanced drying of the Tengger desert, northwest margin of East Asian summer monsoon during warming interglacials after 500 ka. *Quat. Sci. Rev.* **2022**, *293*, 107735. [[CrossRef](#)]
4. Lu, R.J.; Jia, F.F.; Gao, S.Y.; Shang, Y.; Li, J.F.; Zhao, C. Holocene aeolian activity and climatic change in Qinghai Lake basin, northeastern Qinghai-Tibetan Plateau. *Palaeogeogr. Palaeoclimatol. Palaeoecol.* **2015**, *430*, 1–10. [[CrossRef](#)]
5. Zhang, C.L.; Shen, Y.P.; Li, Q.; Jia, W.R.; Li, J.; Wang, X.S. Sediment grain-size characteristics and relevant correlations to the aeolian environment in China's eastern desert region. *Sci. Total Environ.* **2018**, *627*, 586–599. [[CrossRef](#)]
6. Liu, B.; Sun, A.J.; Zhao, H.; Fan, Y.X.; Yang, L.H.; Li, Y.; Li, S.; Wang, K.Q. Physicochemical properties of surface sediments in the Taklimakan desert, northwestern China, and their relationship with oasis–desert evolution. *Catena* **2022**, *208*, 105751. [[CrossRef](#)]
7. Wen, Y.L.; Wu, Y.Q.; Tan, L.H.; Li, D.W.; Fu, T.Y. End-member modeling of the grain size record of loess in the Mu Us Desert and implications for dust sources. *Quat. Int.* **2019**, *532*, 87–97. [[CrossRef](#)]
8. Cheng, L.Q.; Song, Y.G.; Chang, H.; Li, Y.; Orozbaev, R.; Zeng, M.X.; Liu, H.F. Heavy mineral assemblages and sedimentation rates of eastern Central Asian loess: Paleoenvironmental implications. *Palaeogeogr. Palaeoclimatol. Palaeoecol.* **2020**, *551*, 1097. [[CrossRef](#)]
9. Liang, A.M.; Dong, Z.B.; Su, Z.Z.; Qu, J.J.; Zhang, Z.C.; Qian, G.Q.; Wu, B.; Gao, J.L.; Yang, Z.L.; Zhang, C.X. Provenance and transport process for interdune sands in the Kumtagh Sand Sea, Northwest China. *Geomorphology* **2020**, *367*, 107310. [[CrossRef](#)]
10. Li, J.Y.; Dong, Z.B.; Zhang, Z.C.; Qian, G.Q.; Luo, W.Y.; Lu, J.F. Grain-size characteristics of linear dunes on the northern margin of Qarhan Salt Lake, northwestern China. *J. Arid. Land* **2015**, *7*, 438–449. [[CrossRef](#)]
11. Yang, Z.L.; Qian, G.Q.; Han, Z.W.; Dong, Z.B.; Luo, W.Y.; Zhang, Z.C.; Lu, J.F.; Liang, A.M.; Tian, M. Variation in grain-size characteristics as a function of wind direction and height in the Sanlongsha dune field of the northern Kumtagh Desert, China. *Aeolian Res.* **2019**, *40*, 53–64. [[CrossRef](#)]
12. Wang, Q.S.; Song, Y.G.; Duan, L.Q.; Li, J.C. Sensitive Grain-Size Components of Last Glacial Loess on Chinese Loess Plateau and Their Response to East Asian Winter Monsoon. *Atmosphere* **2023**, *14*, 304. [[CrossRef](#)]
13. Folk, R.L.; Ward, W.C. Brazos River Bar: A study in the significance of grain size parameters. *J. Sediment. Res.* **1957**, *27*, 3–26. [[CrossRef](#)]
14. Ashley, G.M. Interpretation of polymodal sediments. *J. Geol.* **1978**, *86*, 411–421. [[CrossRef](#)]
15. Bagnold, R.A.; Barndorff-Nielsen, O. The pattern of natural size distributions. *Sedimentology* **1980**, *27*, 199–207. [[CrossRef](#)]
16. Peng, J.; Wang, X.L.; Zhao, H.; Dong, Z.B. Single-sample unmixing and parametric end-member modelling of grain-size distributions with transformed probability density functions and their performance comparison using aeolian sediments. *Sediment. Geol.* **2023**, *445*, 106328. [[CrossRef](#)]
17. Qiang, M.R.; Chen, F.H.; Wang, Z.T.; Niu, G.M.; Song, L. Aeolian deposits at the southeastern margin of the Tengger Desert (China): Implications for surface wind strength in the Asian dust source area over the past 20,000 years. *Palaeogeogr. Palaeoclimatol. Palaeoecol.* **2010**, *286*, 66–80. [[CrossRef](#)]
18. Xu, S.J.; Pan, B.T.; Gao, H.S.; Gao, G.J.; Su, H. Changes in sand fractions of Binggou section and the expansion and contraction of the Tengger Desert during 50–30 ka. *Earth Surf. Process. Landf.* **2007**, *32*, 475–480.
19. Zhang, Z.C.; Dong, Z.B. Characteristics of dust deposition and particle size in spring in the southeastern Tengger Desert. *China Environ. Sci.* **2011**, *31*, 1789–1794. (In Chinese)
20. Guan, Q.Y.; Zhang, J.D.; Wang, L.J.; Pan, B.T.; Gui, H.J.; Zhang, C. Discussion of the relationship between dustfall grain size and the desert border, taking the southern border of the Tengger Desert and the southern dust deposit area as an example. *Palaeogeogr. Palaeoclimatol. Palaeoecol.* **2013**, *386*, 1–7. [[CrossRef](#)]
21. Zhang, Z.C.; Dong, Z.B.; Li, J.Y. Grain-size characteristics of dune networks in China's Tengger Desert. *Geogr. Ann.* **2015**, *97*, 681–694. [[CrossRef](#)]
22. Peng, J.; Zhao, H.; Dong, Z.B.; Zhang, Z.C.; Yang, H.Y.; Wang, X.L. Numerical methodologies and tools for efficient and flexible unmixing of single-sample grain-size distributions: Application to late Quaternary aeolian sediments from the desert-loess transition zone of the Tengger Desert. *Sediment. Geol.* **2022**, *438*, 106211. [[CrossRef](#)]
23. Liu, B.; Zhao, H.; Yang, F.; Liang, A.M.; Sun, A.J.; Niu, Q.H.; Li, S. A new aeolian activity proxy based on analysis of the grain size characteristics of surface soils across the Tengger Desert, northwest China, and its application to a Quaternary aeolian succession. *Palaeogeogr. Palaeoclimatol. Palaeoecol.* **2023**, *622*, 111594. [[CrossRef](#)]
24. Peng, J.; Wang, X.L.; Yin, G.M.; Adamic, G.; Du, J.H.; Zhao, H.; Kang, S.G.; Hu, G.Y.; Zheng, Y. Accumulation of aeolian sediments around the Tengger Desert during the late Quaternary and its implications on interpreting chronostratigraphic records from drylands in north China. *Quat. Sci. Rev.* **2022**, *275*, 107288. [[CrossRef](#)]
25. Peng, J.; Dong, Z.B.; Han, F.Q.; Gao, L. Aeolian activity in the south margin of the Tengger Desert in northern China since the Late Glacial Period revealed by luminescence chronology. *Palaeogeogr. Palaeoclimatol. Palaeoecol.* **2016**, *457*, 330–341. [[CrossRef](#)]
26. Friedman, G.M.; Sanders, J.E. *Principles of Sedimentology*; Wiley: New York, NY, USA, 1978.
27. Balian, H.G.; Eddy, N.W. Figure-of-merit (FOM), an improved criterion over the normalized chi-squared test for assessing goodness-of-fit of gamma-ray spectral peaks. *Nucl. Instrum. Methods* **1977**, *145*, 389–395. [[CrossRef](#)]

28. Galbraith, R.F.; Green, P.F. Estimating the component ages in a finite mixture. *Nucl. Tracks Radiat. Meas.* **1990**, *17*, 197–206. [[CrossRef](#)]
29. Schwarz, G. Estimating the dimension of a model. *Ann. Stat.* **1978**, *6*, 461–464. [[CrossRef](#)]
30. Weltje, G.J. End-member modeling of compositional data: Numerical-statistical algorithms for solving the explicit mixing problem. *Math. Geol.* **1997**, *29*, 503–549. [[CrossRef](#)]
31. Galbraith, F.R. Graphical Display of Estimates Having Differing Standard Errors. *Technometrics* **1988**, *30*, 271–281. [[CrossRef](#)]
32. Sun, D.H.; Bloemendal, J.; Rea, D.K.; Vandenberghe, J.; Jiang, F.C.; An, Z.S.; Su, R.X. Grain-size distribution function of polymodal sediments in hydraulic and aeolian environments, and numerical partitioning of the sedimentary components. *Sediment. Geol.* **2002**, *152*, 263–277. [[CrossRef](#)]
33. Li, S.; Yang, S.L.; Liang, M.H.; Cheng, T.; Chen, H.; Liu, N.N. The End Member Model Analysis on Grain Size of Loess in the Eastern Tibetan Plateau. *Earth Environ.* **2018**, *46*, 331–338. (In Chinese)
34. Chen, F.H.; Chen, S.Q.; Zhang, X.; Chen, J.H.; Wang, X.; Gowan, E.J.; Qiang, M.R.; Dong, G.H.; Wang, Z.L.; Li, Y.C.; et al. Asian dust-storm activity dominated by chinese dynasty changes since 2000 BP. *Nat. Commun.* **2020**, *11*, 992. [[CrossRef](#)]
35. Wu, P.; Xie, Y.Y.; Li, Y.; Kang, C.G.; Chi, Y.P.; Sun, L.; Wei, Z.Y. Provenance variations of the loess deposits in the East Asian monsoon boundary zone, Northeast China: Response to the variations of climate and wind regimes. *Catena* **2023**, *222*, 106804. [[CrossRef](#)]
36. Crouvi, O.; Amit, R.; Enzel, Y.; Porat, N.; Sandler, A. Sand dunes as a major proximal dust source for late Pleistocene loess in the Negev Desert, Israel. *Quat. Res.* **2008**, *70*, 275–282. [[CrossRef](#)]
37. Amit, R.; Enzel, Y.; Mushkin, A.; Gillespie, A.; Batbaatar, J.; Crouvi, O.; Vandenberghe, J.; An, Z. Linking coarse silt production in Asian sand deserts and Quaternary accretion of the Chinese Loess Plateau. *Geology* **2014**, *42*, 23–26. [[CrossRef](#)]
38. Swet, N.; Kok, F.J.; Huang, Y.; Yizhaq, H.; Katra, I. Low Dust Generation Potential From Active Sand Grains by Wind Abrasion. *J. Geophys. Res. Earth Surf.* **2020**, *125*, e2020JF005545. [[CrossRef](#)]
39. Wu, G.J.; Pan, B.T.; Li, J.J.; Guan, Q.Y.; Liu, Z.G. Tectonic-climatic events in eastern Qilian Mountains over the past 0.83 Ma. *Sci. China* **2001**, *44*, 251–260. [[CrossRef](#)]
40. Pan, B.T.; Wu, G.J.; Wang, Y.X.; Liu, Z.G.; Guan, Q.Y. Age and genesis of the Shagou River terraces in eastern Qi-lian Mountains. *Chin. Sci. Bull.* **2001**, *46*, 509–513. [[CrossRef](#)]
41. Derbyshire, E.; Meng, X.M.; Kemp, R.A. Provenance, transport and characteristics of modern aeolian dust in western Gansu Province, China, and interpretation of the Quaternary loess record. *Arid Environ.* **1998**, *39*, 497–516. [[CrossRef](#)]
42. Stevens, T.; Palk, C.; Carter, A.; Lu, H.Y.; Clift, P.D. Assessing the provenance of loess and desert sediments in northern China using U-Pb dating and morphology of detrital zircons. *Geol. Soc. Am. Bull.* **2010**, *122*, 1331–1344. [[CrossRef](#)]
43. Zhang, H.B.; Nie, J.S.; Liu, X.J.; Pullen, A.; Li, G.Q.; Peng, W.B.; Zhang, H.Z. Spatially variable provenance of the Chinese Loess Plateau. *Geology* **2021**, *49*, 1155–1159. [[CrossRef](#)]
44. Ding, Z.L.; Sun, J.M.; Rutter, N.W.; Rokosh, D.; Liu, T.S. Changes in sand content of loess deposits along a north–south transect of the Chinese Loess Plateau and the implications for desert variations. *Quat. Res.* **1999**, *52*, 56–62. [[CrossRef](#)]
45. Amit, R.; Enzel, Y.; Crouvi, O. Quaternary influx of proximal coarse-grained dust altered circum-Mediterranean soil productivity and impacted early human culture. *Geology* **2021**, *49*, 61–65. [[CrossRef](#)]
46. Roskin, J.; Katra, I.; Blumberg, D.G. Particle-size fractionation of eolian sand along the Sinai–Negev erg of Egypt and Israel. *Geol. Soc. Am. Bull.* **2014**, *126*, 47–65. [[CrossRef](#)]
47. Vandenberghe, J.; Sun, Y.; Wang, X.; Abels, H.A.; Liu, X. Grain-size characterization of reworked fine-grained aeolian deposits. *Earth-Sci. Rev.* **2018**, *177*, 43–52. [[CrossRef](#)]
48. Pye, K. *Aeolian Dust and Dust Depositions*; Academic Press: London, UK, 1987.
49. Lin, Y.C.; Mu, G.J.; Xu, L.S.; Zhao, X. The origin of bimodal grain-size distribution for aeolian deposits. *Aeolian Res.* **2016**, *20*, 80–88. [[CrossRef](#)]
50. Lv, P.; Dong, Z.B.; Zhang, Z.C.; Zhao, A.G. Characteristics of wind velocity, temperature and humidity profiles of near-surface layer in Tengger desert. *J. Desert Res.* **2009**, *29*, 977–981. (In Chinese)
51. Guan, Q.Y.; Pan, B.T.; Li, N.; Li, Q.; Zhang, J.D.; Xu, S.J.; Gao, H.S.; Liu, J. Loess record of the evolution history of severe sandstorms in the Tengger Desert during the Last Interglacial Period (MIS5). *Geosci. J.* **2010**, *14*, 155–162. [[CrossRef](#)]
52. Sun, Y.B.; Clemens, S.C.; Morrill, C.; Lin, X.P.; Wang, X.L.; An, Z.S. Influence of Atlantic meridional overturning circulation on the East Asian winter monsoon. *Nat. Geosci.* **2012**, *5*, 46–49. [[CrossRef](#)]

**Disclaimer/Publisher’s Note:** The statements, opinions and data contained in all publications are solely those of the individual author(s) and contributor(s) and not of MDPI and/or the editor(s). MDPI and/or the editor(s) disclaim responsibility for any injury to people or property resulting from any ideas, methods, instructions or products referred to in the content.